atmosphere

MDPI

Article

Evapotranspiration Estimation Using Remote Sensing Technology Based on a SEBAL Model in the Upper Reaches of the Huaihe River Basin

Linshan Tan [1,2], Kaiyuan Zheng [2,3], Qiangqiang Zhao [1] and Yanjuan Wu [1,2,3,*]

[1] Department of Geography and Spatial Information Techniques, Ningbo University, Ningbo 315211, China; 1911073012@edu.nbu.cn (L.T.); 1811073022@nbu.edu.cn (Q.Z.)
[2] Ningbo Universities Collaborative Innovation Center for Land and Marine Spatial Utilization and Governance Research, Ningbo University, Ningbo 315211, China; 1911073023@edu.nbu.cn
[3] Institute of East China Sea, Ningbo University, Ningbo 315211, China
* Correspondence: wuyanjuanfree@sina.cn

Abstract: Understanding the spatial and temporal variations of evapotranspiration (*ET*) is vital for water resources planning and management and drought monitoring. The development of a satellite remote sensing technique is described to provide insight into the estimation of *ET* at a regional scale. In this study, the Surface Energy Balance Algorithm for Land (SEBAL) was used to calculate the actual *ET* on a daily scale from Landsat-8 data and daily ground-based meteorological data in the upper reaches of Huaihe River on 20 November 2013, 16 April 2015 and 23 March 2018. In order to evaluate the performance of the SEBAL model, the daily SEBAL *ET* (ET_{SEBAL}) was compared against the daily reference *ET* (ET_0) from four theoretical methods: the Penman-Monteith (P-M), Irmak-Allen (I-A), the Turc, and Jensen-Haise (J-H) method, the ET_{MOD16} product from the MODerate Resolution Imaging Spectrometer (MOD16) and the ET_{VIC} from Variable Infiltration Capacity Model (VIC). A linear regression equation and statistical indices were used to model performance evaluation. The results showed that the daily ET_{SEBAL} correlated very well with the ET_0, ET_{MOD16}, and ET_{VIC}, and bias between the ET_{SEBAL} with them was less than 1.5%. In general, the SEBAL model could provide good estimations in daily *ET* over the study region. In addition, the spatial-temporal distribution of ET_{SEBAL} was explored. The variation of ET_{SEBAL} was significant in seasons with high values during the growth period of vegetation in March and April and low values in November. Spatially, the daily ET_{SEBAL} values in the mountain area were much higher than those in the plain areas over the study region. The variability of ET_{SEBAL} in this study area was positively correlated with elevation and negatively correlated with surface reflectance, which implies that elevation and surface reflectance are the important factors for predicting *ET* in this study area.

Keywords: evapotranspiration; Huaihe River Basin; SEBAL model; spatial distribution

Citation: Tan, L.; Zheng, K.; Zhao, Q.; Wu, Y. Evapotranspiration Estimation Using Remote Sensing Technology Based on a SEBAL Model in the Upper Reaches of the Huaihe River Basin. *Atmosphere* **2021**, *12*, 1599. https://doi.org/10.3390/atmos12121599

Academic Editors: Jianyu Liu, Yulong Zhong, Yuqing Zhang and Tingting Ning

Received: 3 November 2021
Accepted: 27 November 2021
Published: 30 November 2021

1. Introduction

Surface evapotranspiration (*ET*) as a crucial part of energy transfer, has an important impact on the growth and development of plant roots [1,2]. *ET* in this case becomes an important implication for drought monitoring and assessment for large areas and, particularly, irrigated agricultural areas [3]. Global warming leads to changes in the hydrological cycle, which lead to the rise in frequency of drought and floods [4]. The Huaihe River Basin (HRB) is an area affected severely by drought, and is very important crop-producing area of China. The reliable and consistent estimation of spatial and temporal distribution of *ET* over this region is of great importance in managing water resources for crops.

Since direct measurement of *ET* is time consuming, costly and difficult, traditionally, *ET* was estimated indirectly from climatic variables such as solar radiation, air temperature,

wind speed, and relative humidity at meteorological stations [5,6]. A number of methods are available for *ET* estimation. The Penman-Monteith (P-M) equation [7] as reported by Allen has been widely used to estimate grass *ET* under different climatic conditions and also adopted as the standard method for definition and computation of *ET* [8]. Using the P-M equation, Djaman et al. [9] estimated the grass-reference *ET* in Sahelian conditions and indicated that its performance was not good when only temperature data is available. Sensitivity of P-M method in estimating *ET* with climatic variables for different climate regions in India was examined by Debnath [10], and results showed that the sensitivity of *ET* to the climate variables had considerable spatial and temporal variation. This method requires a full climate dataset that is not always available at all weather stations, especially in most of the developing countries. In recent years, the water balance method has been widely used for estimation of basin-scale *ET*. For example, using the water balance method, Liu et al. [11] calculated the reference annual *ET* for 35 global river basins to evaluate the performance of nine products in *ET* estimation. Xue et al. [12] estimated *ET* with the water balance method for the upper Yellow River and Yangtze River basins on the Tibetan Plateau. The Turc equation is another one of the simplest empirical equations used to calculate reference *ET* under humid conditions [13]. However, this method generally underestimates *ET* values at windy humid locations while overestimates *ET* at windless humid locations. Other methods such as the Priestley-Taylor method, Irmak-Allen method, and Jensen-Haise method (J-H) have been widely used in previous studies to estimate the *ET* over different regions in the world [14–16]. However, due to the difficulties in gathering all of the necessary climate variables, and the sparse network of point observations can present serious limitations for these methods.

In addition, *ET* has high spatial heterogeneity and temporal variability due to the wide spatial variability of its factors, such as precipitation, solar radiation, air temperature, hydraulic characteristics of soils, elevation, surface temperature, and vegetation types [17]. Groundwater evaporation and soil evaporation are the main sources of *ET* [18]. Shah et al. [19] proposed that nearly all *ET* was from the surface within 0.5 m. *ET* is the main mechanism of groundwater consumption [20], and an exponential relationship is more reasonable than a linear one [21]. *ET* is strongly correlated with soil moisture in areas with poor vegetation coverage [22] and is sensitive to temperature, atmospheric humidity, solar radiation and wind speed, and their seasonal variations [23]. Based on this, it is necessary to clarify the characteristics of the natural environment that affect *ET*, and to quantify the correlation between impact factors and *ET* to provide guarantees for agricultural production and food security.

Accurate information on the spatial and temporal variability of *ET* plays a crucial role in integrated water resources planning, development and management, especially in agriculture areas. To address the limitation of *ET* estimation from ground-based observations, a number of global *ET* products have been derived in recent years, including remote sensing-based products. An alternative approach is to estimate *ET* on local, regional and global-scales by combining surface parameters derived from remote sensing data with surface meteorological variables and vegetation characteristics [24]. Different remote sensing sensors on different platforms including Landsat, the Moderate Resolution Imaging Spectroradiometer, the Advanced Very High-Resolution Radiometer, the Visible Infrared Imaging Radiometer Suite, and the Advanced Spaceborne Thermal Emission and Reflection Radiometer can provide multispectral data with various temporal and spatial resolutions to estimate *ET* over large areas [25]. A number of models have been proposed for estimating *ET* by using remotely sensed data, e.g., the Surface Energy Balance Algorithm for Land Model (SEBAL) [25,26], Mapping Evapotranspiration at High Resolution with Internalized Calibration (METRIC) [27], the Simplified Surface Energy Balance Index (SSEBI) [28], the Surface Energy Balance System Model (SEBSM) [29,30], and the Surface Energy Balance Algorithm for Land-Improved (SEBALI) [31,32]. The use of remote sensing to estimate *ET* has been tested successfully in different climate regions of the world. For example, Wagle et al. [33] indicated that SSEBI, SEBAL and SEBS performed reasonably

well for estimating daily *ET* over a high biomass sorghum field during the 2012 and 2013 growing seasons. Xue et al. [34] found the daily RS-based *ET* for crops in the Central Valley of California from METRIC, SEBS and SEBAL models were within acceptable levels of uncertainty and agreed well with surface renewal estimates. Comparing the *ET* derived from the remote sensing-based *ET* estimation models against conventional *ET* estimation techniques, review studies by Karimi and Bastiaanssen [35] indicated that annual and seasonal remote sensing-based *ET* estimates had an acceptable mean absolute percentage error ranging from 1% to 20%, with an average of 6%. SEBALI, an enhanced version of SEBAL, was used to estimate *ET* for different climatic regions in different countries, and results showed it can provide good *ET* estimations [31,32]. Multi-year remote sensing-based global actual *ET* datasets have been produced by combining different algorithms with recent advancements in satellite remote sensing technologies [36]. Examples of such datasets include the Moderate Resolution Imaging Spectrometer (MODIS) MOD16, and this product has been widely used in *ET* assessment at different scales [37,38]. Many land surface hydrological models are also used to estimate *ET*, i.e., the Soil and Water Assessment Tool (SWAT) and Variable Infiltration Capacity (VIC). Jiang et al. [39] demonstrated the success of using the VIC to simulate *ET* in the Loess Plateau.

SEBAL is a physically based *ET* estimation model developed by Bastiaanssen [26] that estimates *ET* across different ecosystems as a term of the instantaneous surface energy balance using remote sensing data and local meteorological data. Moreover, it has fewer requirements for concurrent ground-level observations [40]. In this study, the SEBAL model was applied to estimate the spatial and temporal variation of *ET* in the upper reaches of the Huaihe River Basin. Three Landsat-8 images were used for this purpose, as well as meteorological data. Moreover, four theoretical methods, the Penman-Monteith (P-M), Irmak-Allen (I-A), Turc, and Jensen-Haise methods (J-H) were also used to validate the results of the SEBAL model. In addition, we explored the impacts of the underlying surface and atmospheric environment on spatial distribution of ET_{SEBAL}. The findings provide a scientific basis for rational development and utilization efficiency of water resources in the study region.

2. Materials and Methods

2.1. Study Area

The Huaihe River is an important geographical dividing line in China and a transition belt between southern and northern parts (Figure 1) [41]. The north region of the Huaihe River is located in a warm-temperate zone, and the south is located in a north subtropical zone [42,43], The various soil types are dominated by alfisols, anthrosols, lakes and reservoirs, with primary soil and semi-hydromorphic soil. Hydrothermal conditions play an essential role in the growth of crops, and the overall environment is suitable for the crops to grow on. The field near the Huaihe River Basin (HRB) is fertile mainly yielding wheat, maize, and potatoes, and is one of China's grain production areas [44]. The study area in the upper reaches of the HRB is approximately 3.1×10^4 km^2, surrounded by numerous rivers and tortuous topography.

2.2. Data Source

Data were derived from the National Meteorological Science Data Center (http://data.cma.cn/data/cdcdetail/dataCode/A.0012.0001.html, accessed on 1 July 2020), including daily temperature, precipitation, and wind speed. Geographic data including DEM, and soil types were extracted from the Geospatial Data Cloud Platform of the Chinese Academy of Sciences (http://www.gscloud.cn, accessed on 5 March 2020) and the Food and Agriculture Organization of the United Nations, FAO (http://www.fao.org/home/zh/, accessed on 29 June 2020). Landsat-8 satellite remote sensing data (Table 1) were downloaded from the Geospatial Data Cloud (http://www.gscloud.cn, accessed on 30 June 2020) for operation of SEBAL. The results of the atmospheric scattering correction were tested before the calculation. Two remote sensing images were mosaiced together to generate the final image

for the study area and the percentage of cloud cover area for each remote sensing image on a given day was calculated (Table 1).

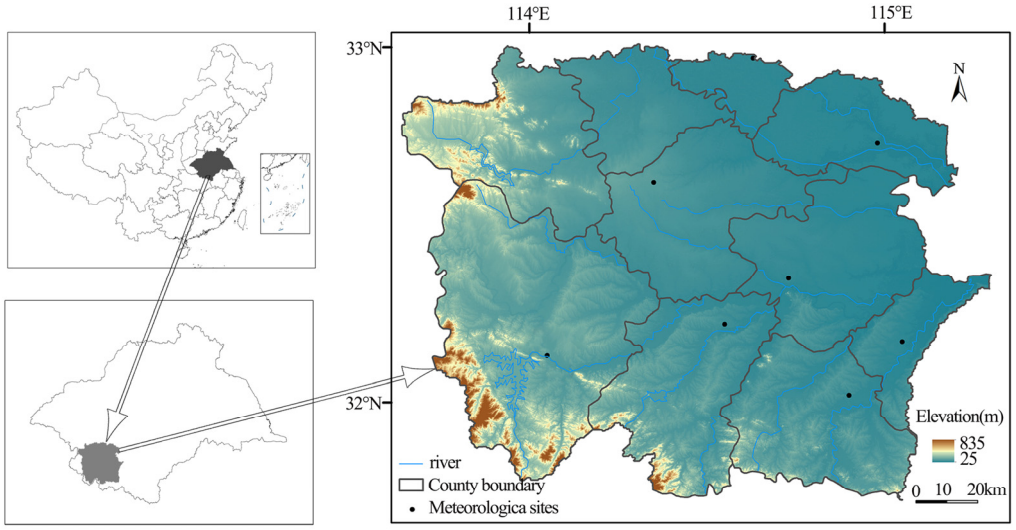

Figure 1. Study area location and elevation and meteorological stations.

Table 1. Data information of Landsat-8.

Date	Ordinal Numbers	Orbit Number	Line Number	Cloud Cover (%)
20 November 2013	324d	123	37	2.23
		123	38	0.13
16 April 2015	106d	123	37	3.14
		123	38	1.31
23 March 2018	83d	123	37	1.14
		123	38	0.54

A remote-sensing *ET* product from the MODerate Resolution Imaging Spectrometer (MOD16) downloaded from Google Earth Engine (https://developers.google.com/earth-engine/datasets/catalog/MODIS_006_MOD16, accessed on 19 November 2021) was also used in this study. MOD16 is a global terrestrial *ET* from earth land surface that represents all evaporation from the soil and wet surfaces, as well as the transpiration from vegetation. The MOD16 *ET* (ET_{MOD16}) datasets were estimated using Mu et al. [37] with an improved *ET* algorithm over the previous Mu et al. [45] paper. The algorithm used for the ET_{MOD16} is based on the Penman-Monteith(P-M) equation [46,47]. *ET* simulated from Variable Infiltration Capacity (ET_{VIC}) for eight stations used in this study was calculated by Luo, and the details of the calculation of the ET_{VIC} can be found in Luo's thesis [48].

2.3. Method

2.3.1. Calculation and Calibration of Each Component in the SEBAL Model

Using a Surface Energy Balance Algorithm for Land (SEBAL) algorithm to estimate the *ET* has obtained high accuracy in many case studies, and is currently the most reasonable and accurate method of estimating surface *ET* [49,50]. Zwart et al. [51] proposed SEBAL based on an equation of surface energy balance as follows:

$$R_n = H + G + \lambda ET \quad (1)$$

where H is sensible heat flux, λ is the coefficient of latent heat in water vaporization, R_n is the net radiation, G means the soil heat flux, and λET is the latent heat flux. Remote sensing data obtained were recorded instantaneously, so the time format of *ET* is instantaneous.

Daily ET in 24 h was calculated by the equation ($F = R_n - G$) because the ratio of ET was constant.

Parameter Adjustment of Surface Net Radiation (R_n)

Equations for surface net radiation are as follows:

$$R_n = (1-a)R_s\downarrow + R_L\downarrow - R_L\uparrow - (1-e)R_L\downarrow \quad (2)$$

$$R_s = \frac{G_{SC} \times cos(\theta) \times t_{sw}}{dr^2} \quad (3)$$

$$R_L\downarrow = \varepsilon_a \sigma T_a^4 \quad (4)$$

$$R_L\uparrow = esT_s^4 \quad (5)$$

$$\varepsilon_a = 1.08(-ln\tau_{sw})^{0.265} \quad (6)$$

$$T_a = 16.0110 + 0.9261T_{air} \quad (7)$$

where α is the surface reflectance, $R_s\downarrow$ is the downward solar radiation, $R_L\downarrow$ is the downward long-wave radiation, $R_L\uparrow$ is the upward long-wave radiation, G_{SC} is the solar constant (1367 W/m^2), ε is land surface emissivity (W/m^2), s is the value of Stefan-Boltzmann constant which is approximately 5.67 $\times$ 10^{-8} W/m^2/K^4, and T_a is the temperature (K) of kinetics on the object surface. In the equation, the effect of elevation on temperature should be considered in the process of retrieving the surface temperature. The temperature declines 0.6 °C for each 100 m rise in elevation, with the relation $T_S = T_{S1} - 0.6$ DEM. The weight coefficient (C_λ) of bands was used to calculate surface reflectance (Table 2).

Table 2. Weight coefficients of Landsat 8 bands.

Band	1	2	3	4	5	7
Weight coefficient	0.2934	0.2736	0.2326	0.1551	0.0325	0.0119

Parameter Adjustment of Soil Heat Flux (G)

While calculating the soil heat flux to simulate the water and heat fluxes, NDVI was used to analyse the bands and extract the basin in study area.

$$G = \frac{T_s - 273.15}{a}[0.0032 \times \frac{a}{c_{11}} + 0.0062 \times (\frac{a}{c_{11}})^2] \times (1 - 0.978NDVI^4) \times R_n \quad (8)$$

where c_{11} is the effect of satellite crossing time on soil heat flux. If the satellite passes overhead at 12:00, the value of c_{11} should be 0.9. The values of c_{11} are 1.0 and 1.1 respectively when the satellite crossing time is in the range of 12:00–14:00 and 14:00–16:00.

Sensible Heat Flux

Sensible heat flux is derived by:

$$H = \frac{r_{air} \times C_{pair} \times (T_{z_1} - T_{z_2})}{r_{ah}} \quad (9)$$

where r_{air} is air density (k/m^3), C_{pair} is the specific heat of air (1004 J/kg/K), T_{Z_1} is the temperature at height Z_1 (when Z_1 = 0.01 m, it is equivalent to the roughness of bare land), T_{Z_2} is the temperature at Z_2 height (when Z_2 = 2 m, this is the reference level of meteorological data) and r_{ah} is the aerodynamic resistances. (s/m).

Calculation of Daily Evapotranspiration (ET_{24})

Instantaneous evapotranspiration (ET_{inst}) and latent heat flux (λET) in study region were calculated by Equations (1)–(9).

$$\lambda ET = R_n - H - G \tag{10}$$

$$ET_{\text{inst}} = \frac{R_n - H - G}{\lambda} \tag{11}$$

$$ET_{24} = \frac{86400 \times \Lambda_{\text{inst}}(R_{n24} - G_{24})}{\lambda} \tag{12}$$

where $R_{n_{24}}$ is the net radiation in 24 h, G_{24} is total soil heat flux in one day, λ is the latent heat in water vaporization, and Λ_{inst} is the ratio of evapotranspiration.

2.3.2. Calculation Method for Reference Evapotranspiration *ET*

FAO-56 Penman-Monteith Method

The FAO-56 Penman-Monteith approach (P-M) is recommended as the standard method for correctly predicting reference evapotranspiration (ET_0) [8], and is expressed in Equation (13) below:

$$ET_0 = K_c \frac{0.408\Delta(R_n - G)\ \frac{900}{T+273}u_2(e_s - e_a)}{\Delta + (1 + 0.34u_2)} \tag{13}$$

where K_c represents the value for the crop coefficient, e_s is the saturation vapor pressure (kPa), e_a is the actual vapor pressure (kPa), Δ is the slope vapor pressure curve, γ is the psychrometric constant (kPa/°C), and u_2 is the wind speed at 2 m height.

Irmak-Allen Method

The Irmak-Allen approach (I-A) was deduced by the data from humid district in Eastern America.

$$ET_0 = K\ (1 + 0.591R_n + 0.047T) \tag{14}$$

where R_n is the net solar radiation, T is the mean temperature (°C), and the empirical constant of K is 0.489 [52]. The adjusting for the value of K depends on the situation, and was adjusted to *0.2589* in October.

Turc Method

The Turc formula for daily ET calculation is given by Equation (15):

$$ET_0 = K \frac{[23.88 \times \left(0.25 + 0.5\frac{n}{N}\right)R_a + 50] \times T}{(T \times 15)} \tag{15}$$

where n is the actual duration (h) of sunshine in a day, N is the astronomic possible sunshine duration (h), T is the mean daily air temperature (°C), the empirical constant of K is 0.013 [53]. The adjusting for the value of K depends on the different months (Table 3).

Table 3. Adjustment table of evapotranspiration in different months calculated by Turc method.

Month	January	March	April	November
K	0.2589	0.0207	0.0025	0.0017

Jensen-Haise Method

The Jensen-Haise model (J-H) is used in computing ET_0 by sampling and observing the soil, which is based on the Equation (16):

$$ET_0 = K(0.0225T - 0.075) \times 0.408 \times \left(0.25 + 0.5\frac{n}{N}\right)R_a \tag{16}$$

All the variables in the Jensen-Haise method are the same as in the Turc method. The empirical constant of K is 0.87 [54]. The adjusting for the value of K depends on the different months (Table 4).

Table 4. Adjustment table of evapotranspiration in different months calculated by the Jensen-Haise method.

Month	January	March	April	October	November
K	0.830	1.987	1.709	1.187	0.837

Considering the effect of climate in different months, the empirical constant of K in I-A method, Turc method and J-H method used the approach by Qin et al. [55] to build an equation of daily linear regression. The positive multiples of K had to be found to adjust values of K in equations by each month.

2.3.3. Partial Correlation Analysis

A partial correlation coefficient is usually used to quantify the strength and linear direction of the relationship between two variables when conditioning on one or several other variables known as control variables of covariates [56]. A univariate analysis was most likely not appropriate as the variables could be strongly linked to each other [57]. Therefore, a partial correlation analysis was used in this study to investigate the correlation between ET_{SEBAL} and one of the four environment variables after removing the effects of the other three variables.

In this study, ENVI (The Environment for Visualizing Images, EVIS, USA), MATLAB (Matrix & Laboratory, MathWorks, Natick, MA, USA), ArcGIS (ESRI, West Redlands, CA, USA), and SPSS (Statistical Product and Service Solutions, IBM, Palo Alto, San Francisco, CA, USA) software were used. MATLAB was used to construct SEBAL. ArcGIS software and ENVI software were used to process remote senses data. MATLAB and the SPSS software were used for numerical calculation and analysis.

3. Results

3.1. Comparative Analysis of Evapotranspiration Estimation

Daily evapotranspiration values obtained using the SEBAL model (ET_{SEBAL}), VIC model (ET_{VIC}), four theoretical (P-M, I-A, Turc, and J-H) methods (ET_0) and remote sensing ET (ET_{MOD16}) for eight stations on 20 November 2013 (mm/d) over the study region are shown in Table 5, and comparisons for ET_{SEBAL} are made with ET_0, ET_{VIC} and ET_{MOD16} (Table 6). The correlations among ET_0, ET_{VIC} and ET_{MOD16} against the SEBAL model estimates were analyzed using the linear regression equation (Figure 2), where the x axis represents daily ET_{SEBAL} estimated by the SEBAL model the y axis represents the daily ET_0, ET_{VIC} and ET_{MOD16}. The coefficient of determination (R^2) has been widely used to evaluate the goodness of fit of evapotranspiration equations [5]. Intercepts (b) and slopes (a) for the least squared regression analysis were calculated and reported. Moreover, in order to obtain a quantitative evaluation, additional statistical measures, mean bias error (MBE) and root mean square error (RMSE), between ET_{SEBAL} and each four ET_0, ET_{VIC} and ET_{MOD16} values, were calculated (Table 6). MBE describes the bias and the RMSE expresses the average difference. MBE and RMSE values are preferably close to 0.

Table 5. Daily evapotranspiration values from the SEBAL model, VIC model, four theoretical methods and remote sensing *ET* for eight stations on 20 November 2013 (mm/d).

ID	Station	SEBAL	I-A	Turc	J-H	P-M	MOD16	VIC
57292	Pingyu	0.8960	0.9358	0.8955	0.8939	0.8954	0.8631	0.9185
57293	Xincai	0.8995	0.9003	0.8954	0.8938	0.8978	0.8016	1.0917
57295	Zhengyang	0.8272	0.8242	0.7626	0.7612	0.8251	0.9765	0.8173
57296	Xi xian	0.8565	0.8721	0.8505	0.8490	0.8573	0.8217	0.8625
57297	Xinyang	0.8687	0.8682	0.8633	0.8618	0.8754	0.7415	0.8705
57298	Luoshan	0.8228	0.8077	0.8279	0.8264	0.8189	0.7568	0.7625
57299	Guangshan	0.8702	0.8922	0.8775	0.8759	0.8738	0.6975	0.8753
58207	Huangchuan	0.8106	0.8113	0.8193	0.8179	0.8094	0.7125	0.8274

Table 6. Summary statistics of daily ET_{SEBAL} estimated from the SEBAL model against ET_0, ET_{MOD16}, ET_{VIC}.

The Calculation Methods or Source of *ET*	R^2	RMSE (mm/d)	MBE (mm/d)	Slope (a)	Intercept (b)
I-A	0.912	0.0178	−0.0075	1.315	−0.262
Turc	0.732	0.0235	0.0074	1.418	−0.134
J-H	0.732	0.0239	0.0089	1.146	−0.134
P-M	0.991	0.0032	−0.0002	1.036	−0.031
MOD16	0.816	0.1085	−0.0818	0.922	0.0689
VIC	0.850	0.0721	0.0013	1.3896	−0.3247

As demonstrated in Figure 2 and Table 6, the daily ET_{SEBAL} from the SEBAL model correlated very well with ET_0, ET_{VIC} and ET_{MOD16}. According to the regression equation, there were high determination correlation values (R^2) of 0.991 and 0.912 between daily ET_{SEBAL} and ET_0 computed from P-M and I-A methods, respectively, while the R^2 value between ET_{SEBAL} and ET_0 computed from Turc and J-H methods was relatively lower at about 0.732. The R^2 between ET_{SEBAL} and ET_{VIC} (ET_{MOD16}) was 0.816 (0.850), and well correlated as can be seen by slopes close to 1 with low value of intercepts. The slopes (intercepts) were 1.315 (−0.262), 1.418 (−0.134), 1.146 (−0.134) and 1.036 (−0.031) for I-A, Turc, J-H and P-M methods, respectively. The slopes (intercepts) were 0.922 (0.059) and 1.389 (−0.325) for ET_{MOD16} and ET_{VIC}, respectively. In addition, MBE and RMSE were close to 0. The error in daily *ET* estimation by SEBAL was less than 1.5% compared to the four theoretical methods. In general, we can see the SEBAL model provided good estimations in the daily evapotranspiration over the study region.

3.2. Spatio-Temporal Distribution of Daily Surface Evapotranspiration

Understanding the spatial and temporal variations of evapotranspiration is critical for regional hydrology, agricultural water requirements, irrigation planning and water resources management over the study region [58]; thus, the spatio-temporal distribution of ET_{SEBAL} in the study area was analyzed (Figure 3). It can be seen that the values of ET_{SEBAL} over the study region had distinctive seasonal variations. The values of ET_{SEBAL} for the study region were less in winter and higher in spring. The ET_{SEBAL} for the entire region on average was less in November, at 0.84 mm/d, with a spatial range of 0.45 to 1.33 mm/d (Figure 3c,f), higher in March at 1.62 mm/d with a range of 1.28 to 3.03mm/d (Figure 3a,d), and very higher in April at 2.11 mm/d with a range of 0.87 to 3.78 mm/d (Figure 3c,f). The ET_{SEBAL} was great during the growth period of the vegetation. The increase in temperature from November to April may make a contribution to the increase in evapotranspiration from winter (November) to spring (March, April). In terms of spatial patterns, the highest ET_{SEBAL} values were located in the far western and southwestern mountain area, whereas the ET_{SEBAL} values in middle and north of the study region, which are mostly composed of plains, were relatively low. Evapotranspiration exhibited large spatial variability at global and regional scales [59–61], which was affected by multiple factors such as underlying

surfaces and the atmospheric environment [62,63]. The possible influencing factors on the observed characteristics of ET_{SEBAL} over study region are examined in the Section 3.3.

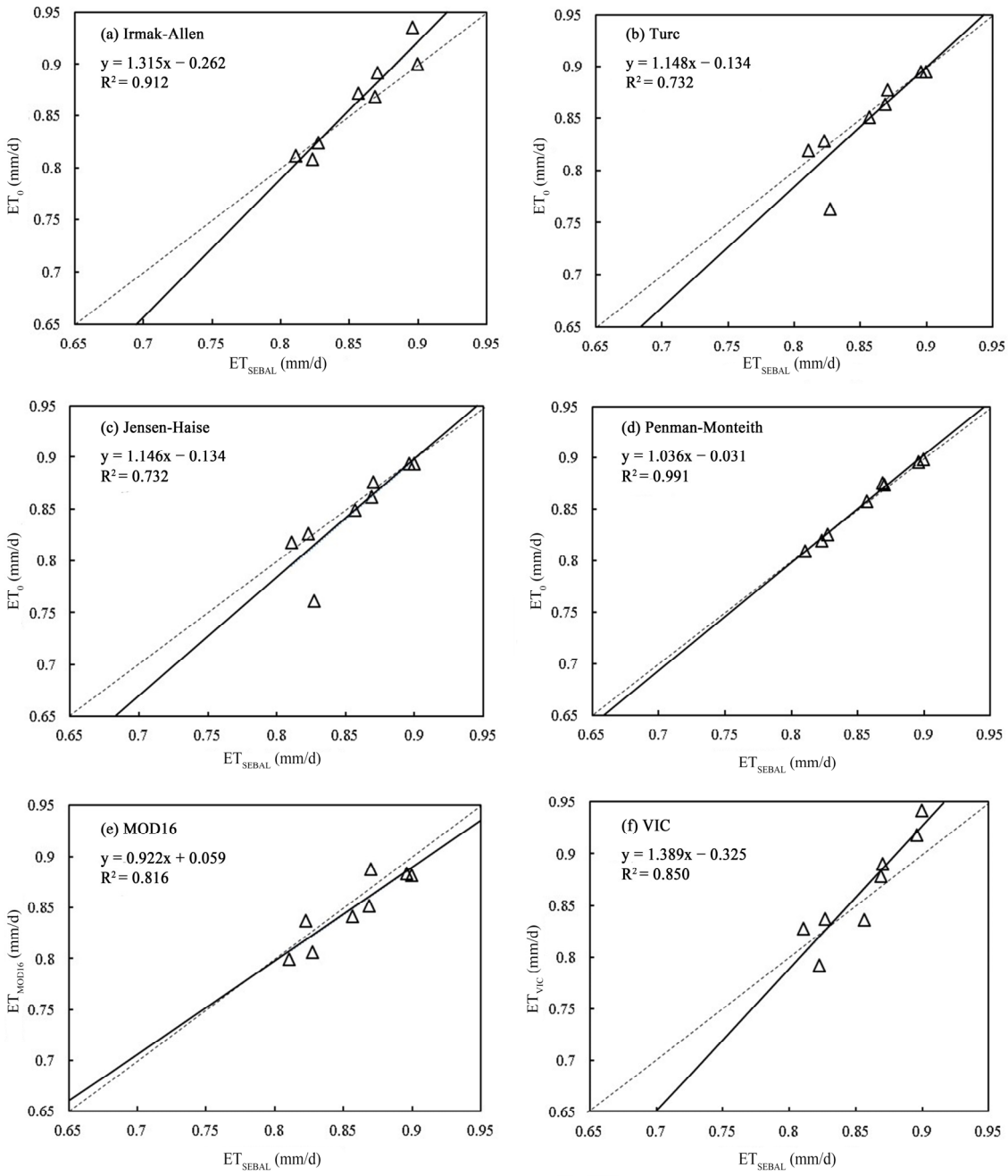

Figure 2. Comparison of daily evapotranspiration from the SEBAL model (ET_{SEBAL}) on 20 November 2013, versus reference evapotranspiration (ET_0) obtained from Imark-Allen (**a**), Turc (**b**), Jensen-Haise (**c**), Penman-Monteith (**d**), ET_{MOD16} (**e**), and ET_{VIC} (**f**). The solid line is the least-squares regression line, and the dashed line is the $x = y$ line.

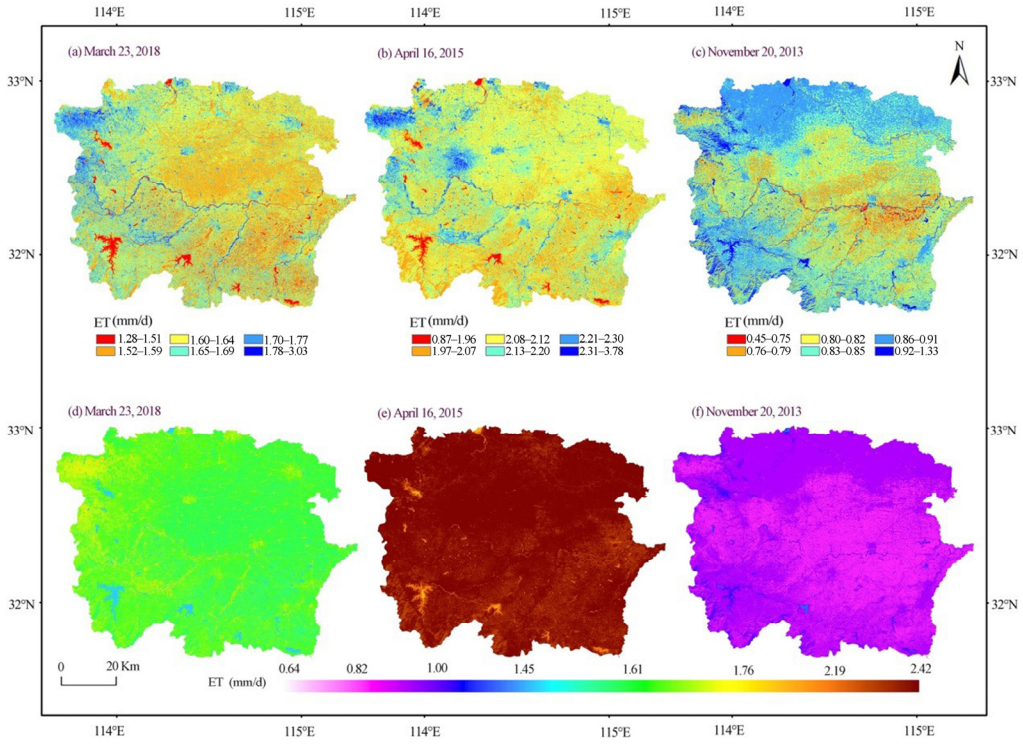

Figure 3. Distribution of daily ET_{SEBAL} over the study region in March 2018 (**a**,**d**), April 2015 (**b**,**e**) and November 2013 (**c**,**f**).

3.3. Influencing Factors of Evapotranspiration

To identify the possible factors that influence daily ET_{SEBAL} over the study region, especially in spatial heterogeneity, a superposition analysis was performed based on *ET* data on March 23, 2018, and raster data of groundwater depths, soil types, elevation, surface temperature, extra-atmospheric reflectance and surface reflectance. The spatial distribution of the ET_{SEBAL} and the groundwater depths is shown in Figure 4. Results show that ET_{SEBAL} was less for the shallowest groundwater depth at 1–3 m, high for the groundwater depth at 3–5 m and higher for the bedrock mountain area. Previous studies had different results in this regard. For example, Huo et al. [19] revealed that evaporation decreased as the water table fell by performing a lysimeter experiment incorporating a 1-year-long bromide tracer test, until it was down to the extinction depth of groundwater. Luo and Sophocleous [64] found that *ET* decreased with increasing depth to the water table through the HYDRUS-1D model in arid and semi-arid regions. In addition, Liu et al. [65] indicated that groundwater depth from 4 to 12 m had little effect on total evaporation in a subtropical scrub forest. Studies have shown that *ET* was also affected by meteorological factors and underlying surface factors [59–61]. The observed characteristics of the ET_{SEBAL} maybe correlated with some of these influencing factors rather than groundwater depth in the study region.

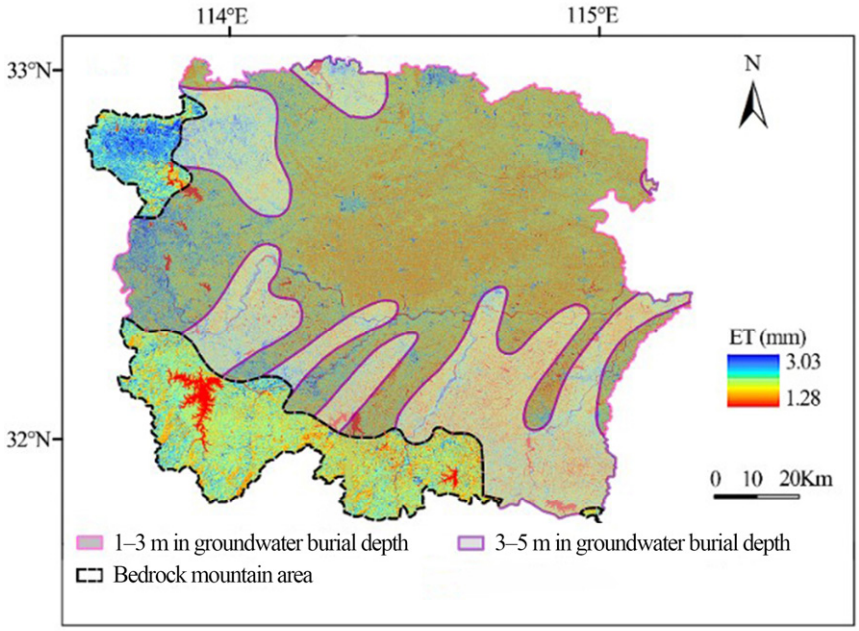

Figure 4. Distribution of daily ET_{SEBAL} and underwater at different depths over the study region in March 2018.

Soil properties directly affect *ET* through changes in sensible heat flux and soil heat flux [49,50]. The spatial distribution of soil types is shown in Figure 5. Five types of soils, including alfisols, semi-hydromorphic soil, anthrosols, primitive and lakes and reservoirs, are recognized in study area. The most common soil types over this region are alfisols, semi-hydromorphic soil and anthrosols, which occupy approximately 42%, 25% and 26% of the study region, respectively. Only 6% and 1% of the study area is occupied by primary soil and lakes and reservoirs (Figure 5 and Table 7). The statistical characteristics of ET_{SEBAL} values are shown in Table 7, and the results reveal that there was no significant difference among these soil types. The mean and median of ET_{SEBAL} value of lakes and reservoirs was 1.459 mm/d and 1.395 mm/d, respectively. The mean (median) of ET_{SEBAL} value was 1.618 mm/d (1.622 mm/d) for alfisols, 1.614 mm/d (1.623 mm/d) for anthrosols and 1.610 mm/d (1.619 mm/d) for semi-hydromorphic soil. The alfisols and semi-hydromorphic soil is mainly concentrated in northwest and northeast of the study region, respectively and anthrosols gathers in the middle of the study region. The mean and median of ET_{SEBAL} value was 1.624 mm/d and 1.626 mm/d for primary soil, which is mostly located at the far western and southwestern mountain area. In general, ET_{SEBAL} value was less for lakes and reservoirs, high for alfisols, anthrosols and semi-hydromorphic soil and higher for primary soil.

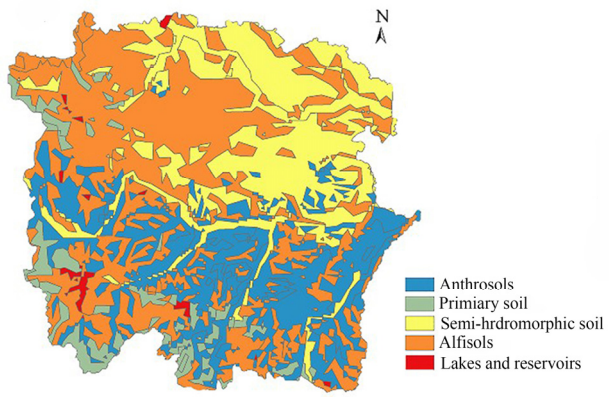

Figure 5. Spatial distribution of different soil types in the study region.

Table 7. Area proportion, mean ET_{SEBAL}, and median ET_{SEBAL} of soil types in the study region.

Area Proportion, Mean *ET*, and Median *ET*	Alfisols	Anthrosols	Lakes and Reservoirs	Primary Soil	Semi-Hydromorphic Soil
Area proportion (%)	42	25	1	6	26
Mean ET_{SEBAL}(mm/d)	1.618	1.614	1.459	1.624	1.610
Median ET_{SEBAL}(mm/d)	1.622	1.623	1.395	1.626	1.619

The relationships between daily ET_{SEBAL} and environment variables, including elevation, surface temperature, extra-atmospheric reflectance and surface reflectance, were also investigated. Partial correlation analysis was used to quantify the correlation between ET_{SEBAL} with one of the environment variables, e.g., elevation, when controlling the other three variables (e.g., surface temperature, extra-atmospheric reflectance and surface reflectance), and the results are shown in Table 8. The partial correlation analysis revealed that elevation, surface temperature, extra-atmospheric reflectance were positively correlated with ET_{SEBAL}, which is consistent with the results of previous research [65,66], while surface reflectance was negatively correlated with ET_{SEBAL}. However, the positive and negative correlations were not statistically significant. The partial correlation between ET_{SEBAL} with elevation was about 0.248, showing that the trend of increasing ET_{SEBAL} with increasing altitude was moderate. There was a slight increase in ET_{SEBAL} with increasing surface temperature and extra-atmospheric reflectance, with a partial correlation of about 0.041 and 0.117, respectively, whereas partial correlation coefficient between surface reflectance and ET_{SEBAL} was −0.534, meaning that an increase in surface reflectance led to a large decrease in ET_{SEBAL}. In general, we can see that the daily ET_{SEBAL} over study region was positively correlated with elevation and negatively correlated with surface reflectance.

Table 8. Partial correlation coefficient between ET_{SEBAL} and elevation, surface temperature, extra-atmospheric reflectance, surface reflectance in the study region.

Influencing Factors	Coefficient	*p*-Value
Elevation	0.248	>0.05
Surface temperature	0.041	>0.05
Extra-atmospheric reflectance	0.117	>0.05
Surface reflectance	−0.534	>0.05

4. Discussion

In this study, the SEBAL model was applied to estimate the characteristics of *ET* in the upper reaches of the Huaihe River Basin, which is in a subtropical zone. Some previous studies have also estimated the *ET* in a subtropical climate area. For example, Rahimikhoob [67] used artificial neural networks to estimate crop evapotranspiration in Iran and found that the neural network provided quite good agreement with the *ET* obtained using the Penman–Monteith method, with an R^2 of 0.95 and a RMSE of 0.41 mm/d. Xu and Singh [68] evaluated the performance of three complementary relationship evapotranspiration models on *ET* estimations in different climatic regions by a water balance approach and found that they were all closely correlated with the water balance calculations with high R^2 values (0.85 in all cases) in the Baixi catchment in Eastern China. Different equations or models were used to estimate *ET*, and different reference *ET*s are chosen as standards for comparison and calibration in the current studies [69], so it is hard to compare the accuracy of *ET* estimations in our study to other studies directly, but the accuracy of the SEBAL in *ET* estimation in this study was considered satisfactory with $R^2 > 0.73$ and small errors. A number of studies have evaluated the performance of the SEBAL model in estimating the *ET* under different climate conditions, and results indicate that SEBAL models have shown reasonable accuracy for predicting *ET* in different parts of the world. For example, Cheng et al. [70] used flux tower observational data to assess

the performance of the SEBAL *ET* and found SEBAL underestimated *ET* in China, with an MBE of −0.15 mm/d.

The SEBAL model was also used to estimate crop evapotranspiration in a maize field in Italy and it was found that the *ET* map from SEBAL largely agreed with the measured yield map, with relative errors of 0.3% among the irrigation management zones and of 1% for the whole field [71]. Teixeira et al. [72] used field measurements to assess the performance of the SEBAL model for estimating *ET* in the semi-arid region of a river basin in Brazil, and results showed that the relation between the SEBAL and field measurements of daily *ET* presented a R^2 of 0.91 and a RMSE of 0.38 mm/d. The SEBAL model *ET* were compared with the Bowen ratio energy balance system-measured fluxes in south-central Nebraska climatic conditions, and results showed that SEBAL can be a viable tool for generating evapotranspiration maps [73]. In general, the SEBAL model can provide a good estimation of *ET*.

However, a bias of SEBAL in *ET* estimation also exits. This may be due to the following reasons. One drawback of SEBAL is that it relies on the presence of extreme instantaneous surface temperature, which requires subjective specifications of representative hot (dry) and cold (wet) pixels in the imagery [40,74]. The selection of hot and cold pixels can have a significant impact on SEBAL *ET* estimation. Second, it always predicts accurate *ET* over flat surfaces, while biases and errors are relatively high when it is applied over mountainous areas [69]. Thus, according to the digital elevation model and the lapse rate, adjustments need to be made to surface temperature. Third, instead of the actual evaporative fraction, the daily integrated *ET* from the SEBAL model was converted from the instantaneous evaporative fraction at the moment of satellite overpass, and the underlying assumption is that the evaporative fraction tends to be constant during the entire day. Fourth, SEBAL is usually used to estimate the *ET* for the cloud-free days across different ecosystems. Liu et al. [74] indicated that even a thin layer of cloud can considerably decrease thermal band readings and cause large errors in calculation of sensible heat fluxes. Future work is required to overcome the above-mentioned issues to improve the performance of SEBAL mode in *ET* estimation.

The spatial heterogeneity of *ET* is considered to be the result of the effects of soil heat flux, net radiation and sensible heat flux in response to the changing underlying surface, climate, and atmospheric environment [59–61]. Obviously, the factors affecting *ET* are different in different climate regions. Shi et al. [75] pointed out that in arid and semi-arid regions, surface temperature, soil moisture content, and thickness of dry sand layers, are considered to affect *ET* by constructing isothermal and non-isothermal models. The value of *ET* in a delta with vigorous vegetation is strongly influenced by groundwater. Due to changes in the depth of groundwater, vegetation changes the absorption capacity of roots through the migration of water in the aeration zone [76]. In China, previous studies have shown that a decrease of wind speed in western and northern China is the main reason for the change in *ET*, the decrease of sunshine duration in subtropical and tropical areas in southern China is the dominant main factor affecting the decrease of annual potential evapotranspiration, and the increase of maximum temperature in cold and temperate regions in northern China is the key factor driving the variation of potential evapotranspiration [77].Based on the regional characteristics of the study region, the underlying surface environment, including elevation, groundwater and soil types, as well as the atmospheric environment, we conducted factor analysis of *ET* spatial heterogeneity. However, it was still difficult to identify the contribution of single factors to evapotranspiration change. Distinguishing dominating features that affect *ET* variation in a region with complex terrain and land use types is a critical step.

5. Conclusions

According to the Landsat-8 data and daily meteorological data from eight stations, the SEBAL model was employed to estimate the daily ET_{SEBAL} in the upper reaches of the HRB. The daily *ET* estimated from the SEBAL model (ET_{SEBAL}) was compared against

the daily reference ET_0 from four (P-M, I-A, Turc, and J-H) methods, ET_{VIC} and ET_{MOD16}. Linear regression and statistical indices of quantitative approaches were used to evaluate the performance of the SEBAL model in *ET* estimation, and results show that the SEBAL model can provide good estimations in daily evapotranspiration over the study area. The SEBAL model is an important tool for spatial and temporal *ET* estimation on a regional scale, which is deemed critical for water resources planning and management.

Considering time scale, ET_{SEBAL} was relatively high during the growth period of the vegetation in March and April, while the ET_{SEBAL} in November was quite low. On the spatial scale, the daily ET_{SEBAL} values in the far western and southwestern mountain area were much higher than those in the plains areas located in the middle and north of study area.

The influence of factors on ET_{SEBAL} was also explored. The ET_{SEBAL} value was relatively high for primary soil located in the mountain area. The daily ET_{SEBAL} over the study area was positively correlated with elevation and negatively correlated with surface reflectance, implying that the variability of ET_{SEBAL} in this study area was affected by elevation and surface reflectance. To make the finding of this study more practical to water resources management, quantitative assessment of the influence of different factors on *ET* should be studied in the future.

Author Contributions: Conceptualization, Y.W.; methodology, K.Z.; software, K.Z.; validation, L.T., K.Z. and Q.Z.; formal analysis, L.T; investigation, Q.Z.; resources, L.T.; data curation, K.Z.; writing—original draft preparation, L.T; writing—review and editing, Y.W. and L.T.; visualization, L.T. and Q.Z.; supervision, Y.W.; project administration, Y.W.; funding acquisition, Y.W. All authors have read and agreed to the published version of the manuscript.

Funding: This research was funded by the National Natural Science Foundation of China (No. 41871024, No. 42001014 and No. 42001025), Humanity and Social Science Youth Foundation of Ministry of Education of China (No. 20YJCZH180), Zhejiang Public Welfare Technology Research (No. LGF21D010003), the Basic Science and Technology Project of Ningbo (No. 202002N3200), Ningbo Fan-3315 Plan, and Leading and Top Tal9ent Training Project of Ningbo.

Data Availability Statement: Data supporting reported results can be found at the National Meteorological Science Data Center (http://data.cma.cn/data/cdcdetail/dataCode/A.0012.0001.html, accessed on 1 July 2020) and Geospatial Data Cloud (http://www.gscloud.cn, accessed on 30 June 2020).

Acknowledgments: The authors thank their cooperative teacher, Chao, G., for invaluable contributions during the process of writing. Constructive comments from anonymous reviewers are greatly appreciated.

Conflicts of Interest: The authors declare that they have no known competing financial interests or personal relationships that could influence the work reported in this paper.

References

1. Gao, C.; Liu, Q.; Su, B.; Zhai, J.; Hu, C. Study on applicability evaluation of hydrological models with different scales and data bases: A case study of Huaihe River Basin. *J. Nat. Resour.* **2013**, *28*, 1765–1777.
2. Wang, K.; Dickinson, R.E. A review of global terrestrial evapotranspiration: Observation, modeling, climatology, and climatic variability. *Rev. Geophys.* **2012**, *50*, 1–54. [CrossRef]
3. Zhao, R.; Wang, H.; Chen, J.; Fu, G.; Zhan, C.; Yang, H. Quantitative analysis of nonlinear climate change impact on drought based on the standardized precipitation and evapotranspiration index. *Ecol. Indic.* **2020**, *121*, 107107. [CrossRef]
4. Huang, S.; Chang, J.; Huang, Q.; Chen, Y. Spatio-temporal changes and frequency analysis of drought in the Wei River Basin, China. *Water Resour. Manag.* **2014**, *28*, 3095–3110. [CrossRef]
5. Efthimiou, N.; Alexandris, S.; Karavitis, C.; Mamassis, N. Comparative analysis of reference evapotranspiration estimation between various methods and the FAO56 Penman-Monteith procedure. *Eur. Water* **2013**, *42*, 19–34.
6. Karimi, P.; Bongani, B.; Blatchford, M.; de Fraiture, C. Global satellite-based ET products for the local level irrigation management: An application of irrigation performance assessment in the Sugarbelt of Swaziland. *Remote Sens.* **2019**, *11*, 705. [CrossRef]
7. Penman, H.L. *Vegetation and Hydrology. Technical Communication NO. 53, Commonwealth Bureau of Soils, Harpenden*; Common-wealth Agricultural Bureaux: Farnham Royal, UK, 1963.
8. Allen, R.G.; Pereira, L.S.; Raes, D.; Smith, M. *Crop Evapotranspiration Guidelines for Computing Crop Water Requirements. Irrigation. Drainage*; Paper. No. 56; FAO: Rome, Italy, 1998.

9. Djaman, K.; Irmak, S.; Kabenge, I.; Futakuchi, K. Evaluation of FAO-56 penman-monteith model with limited data and the valiantzas models for estimating grass-reference evapotranspiration in Sahelian conditions. *J. Irrig. Drain. Eng.* **2016**, *142*, 04016044. [CrossRef]
10. Debnath, S.; Adamala, S.; Raghuwanshi, N.S. Sensitivity analysis of FAO-56 Penman-Monteith method for different agro-ecological regions of India. *Environ. Process.* **2015**, *2*, 689–704. [CrossRef]
11. Liu, W.; Wang, L.; Zhou, J.; Li, Y.; Sun, F.; Fu, G.; Li, X.; Sang, Y.F. A worldwide evaluation of basin-scale evapotranspiration estimates against the water balance method. *J. Hydrol.* **2016**, *538*, 82–95. [CrossRef]
12. Xue, B.L.; Wang, L.; Li, X.; Yang, K.; Chen, D.; Sun, L. Evaluation of evapotranspiration estimates for two river basins on the Tibetan Plateau by a water balance method. *J. Hydrol.* **2013**, *492*, 290–297. [CrossRef]
13. Trajkovic, S.; Kolakovic, S. Wind-adjusted Turc equation for estimating reference evapotranspiration at humid European locations. *Hydrol. Res.* **2009**, *40*, 45–52. [CrossRef]
14. Gao, X.; Peng, S.; Xu, J.; Yang, S.; Wang, W. Proper methods and its calibration for estimating reference evapotranspiration using limited climatic data in Southwestern China. *Arch. Agron. Soil Sci.* **2015**, *61*, 415–426. [CrossRef]
15. Wang, K.; Li, Z.; Cribb, M. Estimation of evaporative fraction from a combination of day and night land surface temperatures and NDVI: A new method to determine the Priestley–Taylor parameter. *Remote Sens. Environ.* **2006**, *102*, 293–305. [CrossRef]
16. Shirmohammadi, A.Z.; Saberali, S.F. Evaluating of eight evapotranspiration estimation methods in arid regions of Iran. *Agric. Water Manag.* **2020**, *239*, 106243. [CrossRef]
17. Abrishamkar, M.; Ahmadi, A. Evapotranspiration Estimation Using Remote Sensing Technology Based on SEBAL Algorithm. *Iran. J. Sci. Technol.* **2016**, *41*, 65–76. [CrossRef]
18. Sanderson, J.S.; Cooper, D.J. Ground water discharge by evapotranspiration in wet-lands of an arid intermountain basin. *J. Hydrol.* **2008**, *351*, 344–359. [CrossRef]
19. Huo, S.Y.; Jin, M.G.; Liang, X.; Li, X.; Hao, H.B. Estimating impacts of water-table depth on groundwater evaporation and recharge using lysimeter measurement data and bromide tracer. *Hydrogeol. J.* **2020**, *28*, 955–971. [CrossRef]
20. Cheng, D.H.; Li, Y.; Chen, X.; Wang, W.K.; Hou, G.C.; Wang, C.L. Estimation of groundwater evapotranspiration using diurnal water table fluctuations in the Mu Us Desert, northern China. *J. Hydrol.* **2013**, *490*, 106–113. [CrossRef]
21. Nyambayo, V.P.; Potts, D.M. Numerical simulation of evapotranspiration using a root water uptake model. *Comput. Geotech.* **2010**, *37*, 175–186. [CrossRef]
22. Bing, L.F.; Su, H.B.; Shao, Q.Q.; Liu, J.Y. Changing characteristic of land surface evapotranspiration and soil moisture in china during the past 30 years. *Geo. Spat. Inf. Sci.* **2012**, *14*, 1–13. [CrossRef]
23. Kul, K.; Izaya, N.; Jeppe, K.; George, V. Dry season evapotranspiration dynamics over human-impacted land-scapes in the Southern Amazon using the Landsat-based METRIC model. *Remote Sens.* **2017**, *9*, 706.
24. Li, Z.L.; Tang, R.; Wan, Z.; Bi, Y.; Zhou, C.; Tang, B.; Yan, G.; Zhang, X. A review of current methodologies for regional evapotranspiration estimation from remotely sensed data. *Sensors* **2009**, *9*, 3801–3853. [CrossRef]
25. Senkondo, W.; Munishi, S.E.; Tumbo, M.; Nobert, J.; Lyon, S.W. Comparing remotely-sensed surface energy balance evapotranspiration estimates in heterogeneous and data-limited regions: A case study of Tanzania's Kilombero Valley. *Remote Sens.* **2019**, *11*, 1289. [CrossRef]
26. Bastiaanssen, W.G.M.; Menenti, M.; Feddes, R.A.; Holtslag, A.A.M. A remote sensing surface energy balance algorithm for land (SEBAL). 1. Formulation. *J. Hydrol.* **1998**, *212–213*, 198–212. [CrossRef]
27. Allen, R.G.; Tasumi, M.; Trezza, R. Satellite-based energy balance for mapping evapotranspiration with internalized calibration (METRIC)—Model. *J. Irrig. Drain. Eng.* **2007**, *133*, 380–394. [CrossRef]
28. Singh, R.K.; Senay, G.B.; Velpuri, N.M.; Bohms, S.; Scott, R.L.; Verdin, J.P. Actual evapotranspiration (water use) assessment of the Colorado River Basin at the Landsat resolution using the operational simplified surface energy balance model. *Remote Sens.* **2014**, *6*, 233–256. [CrossRef]
29. Su, Z. The Surface Energy Balance System (SEBS) for estimation of turbulent heat fluxes. *Hydrol. Earth Syst. Sci.* **2002**, *6*, 85–99. [CrossRef]
30. Sun, H.; Yang, Y.; Wu, R.; Gui, D.; Xue, J.; Liu, Y.; Yan, D. Improving estimation of cropland evapotranspiration by the Bayesian model averaging method with surface energy balance models. *Atmosphere* **2019**, *10*, 188. [CrossRef]
31. Allam, M.; Mhawej, M.; Meng, Q.Y.; Faour, G.; Fadel, A.; Hu, X.L. Monthly 10-m evapo-transpiration rates retrieved by SEBALI with Sentinel-2 and MODIS LST data. *Agric. Water Manag.* **2021**, *243*, 106432. [CrossRef]
32. Mhawej, M.; Nasrallah, A.; Abunnasr YFadel, A.; Faour, G. Better irrigation management using the satellite-based adjusted single crop coefficient (aKc) for over sixty crop types in California, USA. *Agric. Water Manag.* **2021**, *256*, 207059. [CrossRef]
33. Wagle, P.; Bhattarai, N.; Gowda, P.H.; Kakani, V.G. Performance of five surface energy balance models for estimating daily evapotranspiration in high biomass sorghum. *ISPRS J. Photogramm. Remote Sens.* **2017**, *128*, 192–203. [CrossRef]
34. Xue, J.; Bali, K.M.; Light, S.; Hessels, T.; Kisekka, I. Evaluation of remote sensing-based evapotranspiration models against surface renewal in almonds, tomatoes and maize. *Agric. Water Manag.* **2020**, *238*, 106228. [CrossRef]
35. Karimi, P.; Bastiaanssen, W.G.M. Spatial evapotranspiration, rainfall and land use data in water accounting—Part 1: Review of the accuracy of the remote sensing data. *Hydrol. Earth Syst. Sci.* **2015**, *19*, 507–532. [CrossRef]
36. Muhammad, S.K.; Umar, W.L.; Jongjin, B.; Minha, C. Stand-alone uncertainty characterization of GLEAM, GLDAS and MOD16 evapotranspiration products using an extended triple collocation approach. *Agric. For. Meteorol.* **2018**, *252*, 256–268.

37. Mu, Q.; Zhao, M.; Running, S.W. Improvements to a MODIS global terrestrial evapotranspiration algorithm. *Remote Sens. Environ.* **2011**, *115*, 1781–1800. [CrossRef]
38. Jiang, Y.Y.; Wang, W.; Zhou, Z.H. Evaluation of MODIS MOD16 Evapotranspiration Product in Chinese River Basins. *Nat. Resour. J.* **2017**, *32*, 517–528.
39. Jiang, F.X.; Xie, X.H.; Liang, S.L.; Wang, Y.B.; Zhu, B.W.; Zhang, X.T.; Chen, Y.C. Loess Plateau evapotranspiration intensified by land surface radiative forcing associated with ecological restoration. *Agric. For. Meteorol.* **2021**, *331*, 208669. [CrossRef]
40. Jassas, H.; Kanoua, W.; Merkel, B. Actual evapotranspiration in the Al-Khazir Gomal Basin (Northern Iraq) using the surface energy balance algorithm for land (SEBAL) and water balance. *Geosciences* **2015**, *5*, 141–159. [CrossRef]
41. Gao, C.; Ruan, T. Impact of climate change and human activities on Runoff in the middle and upper reaches of the Huaihe River Basin. *J. Geog. Sci.* **2018**, *28*, 79–92. [CrossRef]
42. Gao, C.; Zhang, Z.; Liu, Q.; Ruan, T. An optimal grid method for vulnerability assessment index of disaster bearing body: A case study of rainstorm and flood disaster in the main stream of Huaihe River. *J. Nat. Disasters* **2018**, *27*, 119–129.
43. Gao, C.; Chen, C.; He, Y.; Ruan, T.; Luo, G.; Sun, Y. Response of Agricultural Drought to Meteorological Drought: A Case Study of the Winter Wheat above the Bengbu Sluice in the Huaihe River Basin, China. *Water* **2020**, *12*, 2805. [CrossRef]
44. Gao, C.; Li, X.; Sun, Y.; Zhou, T.; Luo, G.; Chen, C. Water requirement of summer maize at different growth stages and the spatiotemporal characteristics of agricultural drought in the Huaihe River Basin, China. *Theor. Appl. Climatol.* **2019**, *136*, 1289–1302. [CrossRef]
45. Mu, Q.; Heinsch, F.A.; Zhao, M.; Running, S.W. Development of a global evapotranspiration algorithm based on MODIS and global meteorology data. *Remote Sens. Environ.* **2007**, *111*, 519–536. [CrossRef]
46. Allen, R. Penman-Monteith Equation. *Encycl. Soils. Environ.* **2005**, *3*, 180–188.
47. Alexandridis, T.K.; Andrianopoulos, A.; Galanis GKalopesa, E.; Dimitrakos, A.; Katsogiannos, F.; Zalidis, G. An Integrated Approach to Promote Precision Farming as a Measure Toward Reduced-Input Agriculture in Northern Greece Using a Spatial Decision Support System. *Compre. Geo. Inform. Syst.* **2018**, 315–352. [CrossRef]
48. Luo, G. *Research of Water Deficit and Driving Mechanism in Key Growth Stages of Winter Wheat—A Case Study in the Upper Reaches of Huaihe River Basin*; Ningbo University: Ningbo, China, 2020.
49. Zhang, Z.; Li, X.; Liu, L.; Wang, Y.; Li, Y. Influence of mulched drip irrigation on landscape scale evapotranspiration from farmland in an arid area. *Agric. Water Manag.* **2020**, *230*, 105953. [CrossRef]
50. Dos Santos, C.A.C.; Mariano, D.A.; das Chagas, A.; do Nascimento, F.; da CDantas, F.R.; de Oliveira, G.; Silva, M.T.; da Silva, L.L.; da Silva, B.B.; Bezerra, B.G.; et al. Spatio-temporal patterns of energy exchange and evapotranspiration during an intense drought for drylands in Brazil. *Int. J. Appl. Earth Obs. Geoinf.* **2020**, *85*, 101982. [CrossRef]
51. Zwart, S.J.; Bastiaanssen, W.G.M. SEBAL for detecting spatial variation of water productivity and scope for improvement in eight 65 irrigated wheat systems. *Agric. Water Manag.* **2007**, *89*, 287–296. [CrossRef]
52. Irmak, S.; Irmak, A.; Allen, R.G.; Jones, J.W. Solar and net radiationased equations to estimate reference evapotranspiration in humid climates. *J. Irrig. Drain. Eng. ASCE* **2003**, *129*, 336–347. [CrossRef]
53. Turc, L. Estimation of irrigation water requirements, potential evapotranspiration: A simple climatic formula evolved up to date. *Adv. Agron.* **1961**, *12*, 13–49.
54. Jensen, M.E.; Haise, H.R. Estimating evapotranspiration from solar radiation. *J. Irrig. Drain. Div.* **1963**, *89*, 15–41. [CrossRef]
55. Qin, M.; Hao, L.; Shi, T.; Sun, L.; Sun, G. Comparison and improvement of five reference crop evapotranspiration estimation methods in Qinhuai River Basin. *China Agrometeorol.* **2016**, *37*, 390–399.
56. Baba, K.; Shibata, R.; Sibuya, M. Partial correlation and conditional correlation as measures of conditional independence. *Aust. N. Z. J. Stat.* **2004**, *46*, 657–664. [CrossRef]
57. Gao, G.; Chen, D.; Ren GYChen, Y.; Liao, Y.M. Spatial and temporal variations and controlling factors of potential evapotranspiration in China: 1956–2000. *J. Geogr. Sci.* **2006**, *16*, 3–12. [CrossRef]
58. Tabari, H.; Aeini, A.; Talaee, P.H.; Some'e, B.S. Spatial distribution and temporal variation of reference evapotranspiration in arid and semi-arid regions of Iran. *Hydrol. Process.* **2012**, *26*, 500–512. [CrossRef]
59. Maayar, M.M.; Chen, J.M. Spatial scaling of evapotranspiration as affected by heterogeneities in vegetation, topography, and soil texture. *Remotes Sens. Environ.* **2006**, *102*, 33–51. [CrossRef]
60. Joiner, J.; Yoshida, Y.; Anderson, M.; Holmes, T.; Hain, C.; Reichle, R.; Koster, R.; Middleton, E.; Zeng, F.W. Global relationships among traditional reflectance vegetation indices (NDVI and NDII), evapotranspiration (ET), and soil moisture variability on weekly timescales. *Remotes Sens. Environ.* **2018**, *219*, 339–352. [CrossRef]
61. Lehmann, P.; Merlin, O.; Gentine, P.; Or, D. Soil texture effects on surface resistance to bare-soil evaporation. *Geophys. Res. Lett.* **2018**, *45*, 10398–10405. [CrossRef]
62. Su, T.; Feng, G.L. Spatial-temporal variation characteristics of global evaporation revealed by eight reanalyses. *Sci. China Earth Sci.* **2015**, *58*, 255–269. [CrossRef]
63. Howell, T.A.; Evett, S.R.; Tolk, J.A.; Copeland, K.S.; Marek, T.H. Evapotranspiration, water productivity and crop coefficients for irrigated sunflower in the U.S. southern high plains. *Agric. Water Manag.* **2015**, *162*, 33–46. [CrossRef]
64. Luo, Y.; Sophocleous, M. Seasonal groundwater contribution to crop-water use assessed with lysimeter observations and model simulations. *J. Hydrol.* **2010**, *389*, 325–335. [CrossRef]

65. Liu, Y.J.; Chen, J.; Pan, T. Analysis of Changes in Reference Evapotranspiration, Pan Evaporation, and Actual Evapotranspiration and Their Influencing Factors in the North China Plain During 1998–2005. *Earth Space Sci.* **2019**, *6*, 1366–1377. [CrossRef]
66. Xu, Y.; Xu, Y.P.; Wang, Y.F.; Wu, L.; Li, G.; Song, S. Spatial and temporal trends of reference crop evapotranspiration and its influential variables in Yangtze River Delta, eastern China. *Theor. Appl. Climatol.* **2017**, *130*, 945–958. [CrossRef]
67. Rahimikhoob, A. Estimation of evapotranspiration based on only air temperature data using artificial neural networks for a subtropical climate in Iran. *Theor. Appl. Climatol.* **2010**, *101*, 83–91. [CrossRef]
68. Xu, C.Y.; Singh, V.P. Evaluation of three complementary relationship evapotranspiration models by water balance approach to estimate actual regional evapotranspiration in different climatic regions. *J. Hydrol.* **2005**, *308*, 105–121. [CrossRef]
69. Zhong, Y.; Zhong, M.; Mao, Y.; Ji, B. Evaluation of Evapotranspiration for Exorheic Catchments of China during the GRACE Era: From a Water Balance Perspective. *Remote Sens.* **2020**, *12*, 511. [CrossRef]
70. Cheng, M.; Jiao, X.; Li, B.; Yu, X.; Shao, M.; Jin, X. Long time series of daily evapotranspiration in China based on the SEBAL model and multisource images and validation. *Earth Syst. Sci.* **2021**, *13*, 3995–4017. [CrossRef]
71. Gobbo, S.; Lo Presti, S.; Martello, M.; Panunzi, L.; Berti, A.; Morari, F. Inter-grating SEBAL with in-field crop water status measurement for precision irrigation applications-A case study. *Remote Sens.* **2019**, *11*, 2069. [CrossRef]
72. Teixeira, A.D.C.; Bastiaanssen, W.G.; Ahmad, M.; Bos, M.G. Reviewing SEBAL input parameters for assessing evapotranspiration and water productivity for the Low-Middle São Francisco River basin, Brazil: Part B: Application to the regional scale. *Agric. For. Meteorol.* **2009**, *149*, 462–476. [CrossRef]
73. Singh, R.K.; Irmak, A.; Irmak, S.; Martin, D.L. Application of SEBAL model for mapping evapotranspiration and estimating surface energy fluxes in south-central Nebraska. *J. Irrig. Drain. Eng.* **2008**, *134*, 273–285. [CrossRef]
74. Liu, C. Spatial and temporal change in the potential evapotranspiration sensitivity to meteorological factors in China (1960–2007). *J. Geog. Sci.* **2012**, *22*, 3–14. [CrossRef]
75. Shi, T.T.; Guan, D.X.; Wu, J.B.; Wang, A.Z.; An, C.J.J.; Han, S.J. Comparison of methods for estimating evapotranspiration rate of dry forest canopy: Eddy covariance, Bowen ratio energy balance, and Penman-Monteith equation. *J. Geophys. Res.* **2008**, *113*, D19116. [CrossRef]
76. Gao, X.L.; Peng, S.Z.; Wang, W.G.; Xu, J.Z.; Yang, S.L. Spatial and temporal distribution characteristics of reference evapotranspiration trends in Karst area: A case study in Guizhou Province, China. *Meteorol. Atmos. Phys.* **2016**, *128*, 677–688. [CrossRef]
77. Ying, Y.H.; Wang, S.D.; Chen, G.; Dai, E. Attribution analyses of potential evapotranspiration change in China since the 1960s. *Theor. Appl. Climatol.* **2010**, *101*, 19–28.